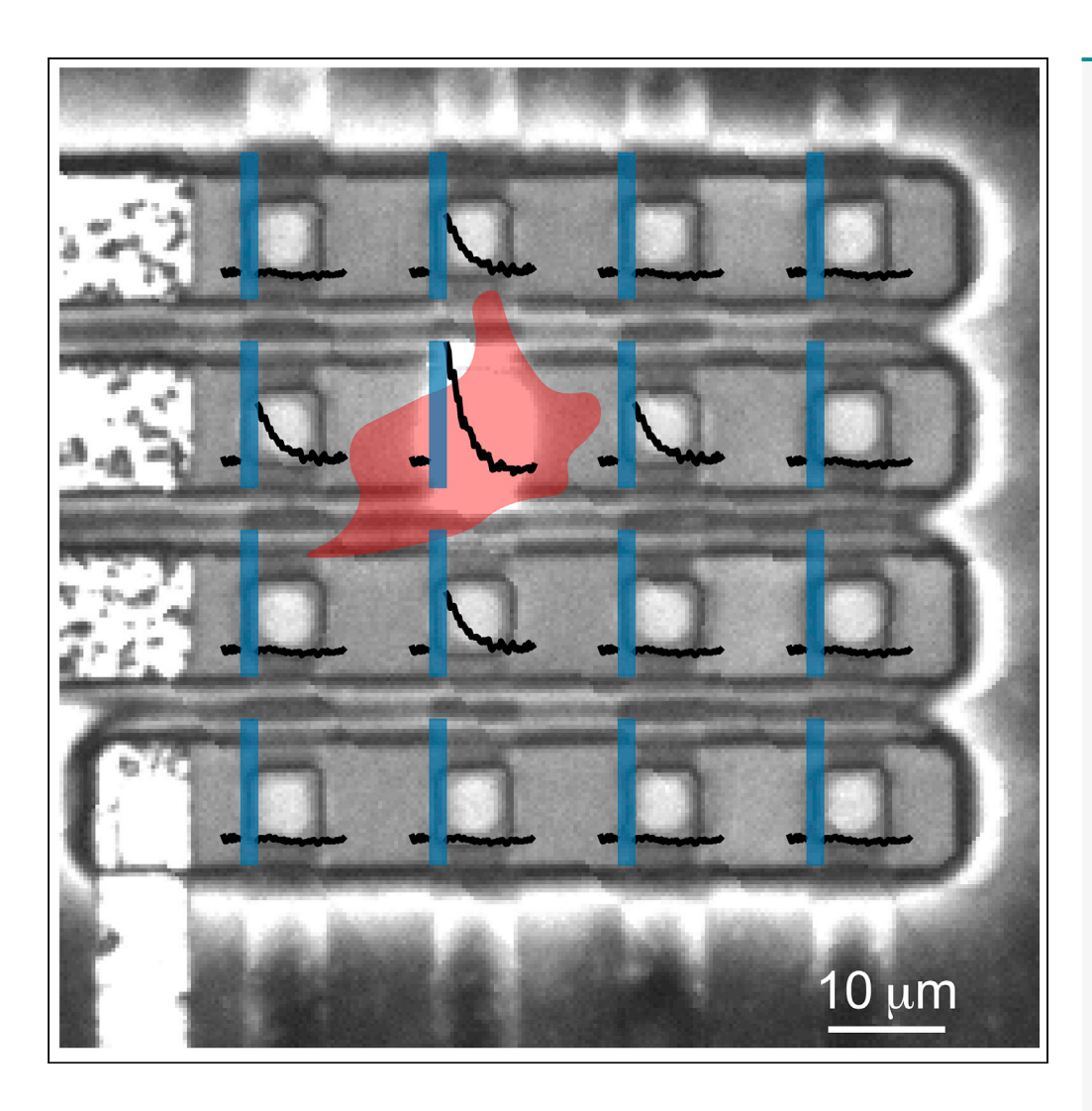


Article

Single-Cell Optogenetic Control of Calcium Signaling with a High-Density Micro-LED Array



Dacheng Mao, Ningwei Li, Zheshun Xiong, Yubing Sun, Guangyu Xu

guangyux@umass.edu (G.X.) ybsun@umass.edu (Y.S.)

HIGHLIGHTS

Precise optogenetic control of Ca²⁺ signaling down to the single cell level

Bright, localized optogenetic stimulus with a high-density micro-LED array

Advancing micro-LED arrays toward a lab-on-achip for single-cell optogenetics

Mao et al., iScience 21, 403–412 November 22, 2019 © 2019 The Author(s). https://doi.org/10.1016/ j.isci.2019.10.024



Article

Single-Cell Optogenetic Control of Calcium Signaling with a High-Density Micro-LED Array

Dacheng Mao, 1,3 Ningwei Li, 2,3 Zheshun Xiong, 1 Yubing Sun, 2,* and Guangyu Xu1,4,*

SUMMARY

Precise optogenetic control, ideally down to single cells in dense cell populations, is essential in understanding the heterogeneity of cell networks. Devices with such capability, if built in a chip scale, will advance optogenetic studies at cellular levels in a variety of experimental settings. Here we demonstrate optogenetic control of intracellular Ca²⁺ dynamics at the single cell level using a 16-µm pitched micro-light emitting diode (LED) array that features high brightness, small spot size, fast response, and low voltage operation. Individual LED pixels are able to reliably trigger intracellular Ca²⁺ transients, confirmed by fluorescence microscopy and control experiments and cross-checked by two genetically coded Ca²⁺ indicators. Importantly, our array can optogenetically address individual cells that are sub-10 µm apart in densely packed cell populations. These results suggest the possible use of the micro-LED array toward a lab-on-a-chip for single-cell optogenetics, which may allow for pharmaceutical screening and fundamental studies on a variety of cell networks.

INTRODUCTION

Over the past decade, optogenetics has emerged as a powerful method to interrogate specific cell types in complex tissues (Boyden, 2015; Deisseroth, 2015). In this method, cells expressed with light-sensitive proteins can be either excited or silenced, when exposed to light pulses at specific wavelengths (Boyden et al., 2005; Prakash et al., 2012). Such bidirectional optical control over the activity of cells enables minimally invasive assessment of their roles at the levels of cells, circuits, and behavior. For these reasons, optogenetics is widely used to modulate the activity of neurons (Chow et al., 2010; Hochbaum et al., 2014), cardiomyocytes (Wang et al., 2017; Johnston et al., 2017), C2C12 myotubes (Asano et al., 2015; Sebille et al., 2017), and human embryonic kidney 293 cells (i.e., HEK 293) (Baaske et al., 2018; Miyazaki et al., 2019), which deepens the understanding of brain/heart/muscle functions and gene expression.

To make the full impact of optogenetics, research has now focused on advancing the hardware to enable precise optogenetic control (McGovern et al., 2010; Nakajima et al., 2012; Steude et al., 2016), ideally down to single cells in dense cell populations. Such single-cell precision is essential in understanding the heterogeneity of cell networks, which is challenging to achieve by electrical stimulation methods using micro/ nanoelectrodes (Hierlemann et al., 2011; Abbott et al., 2017; Lu et al., 2018). If successful, the resulting hardware will help scientists find precise connections within and between different tissue regions at an unprecedented cellular level. However, it is technically difficult to express optogenetic actuators in targeted single cells; in fact, densely packed cells often express them simultaneously, thereby all becoming light sensitive. Thus, to achieve single-cell optogenetic control one should employ high-density light sources that can address individual cells by localized light output.

Among available light sources, micron-sized light-emitting diode arrays (i.e., micro-light emitting diode [LED] arrays) are suitable for high-precision optogenetic control (Steude et al., 2016; Poher et al., 2008; Grossman et al., 2010; McGovern et al., 2010; Nakajima et al., 2012; Pisanello et al., 2016). These devices are recognized for their scalability, good lifetime in biological environments, and medium power dissipation for in vivo use. To date, GaN-based micro-LED arrays with 50- to 200-μm pitches have been built into the microscope optics for multi-site light illumination at a variety of settings, using a patch clamp or microelectrode arrays to record optogenetically induced action potentials (Grossman et al., 2010; Nakajima et al., 2012). Recently, organic micro-LED arrays with sub-10-µm pitches have been applied to HEK 293 cell culture, employing a patch clamp to monitor the photocurrent in single cells that were illuminated by three LED pixels (Steude et al., 2016). Although these studies showcased single-cell optogenetics using high-density micro-LEDs, studying cell activity in the electrical domain only is insufficient to fully understand cellular network dynamics. In fact, cell circuits often not only involve the transmission of electrical ¹Department of Electrical and Computer Engineering. University of Massachusetts, Amherst, MA 01003, USA

²Department of Mechanical and Industrial Engineering, University of Massachusetts, Amherst, MA 01003, USA

³These authors contributed equally

⁴Lead Contact

*Correspondence: guangyux@umass.edu (G.X.), ybsun@umass.edu (Y.S.) https://doi.org/10.1016/j.isci. 2019.10.024



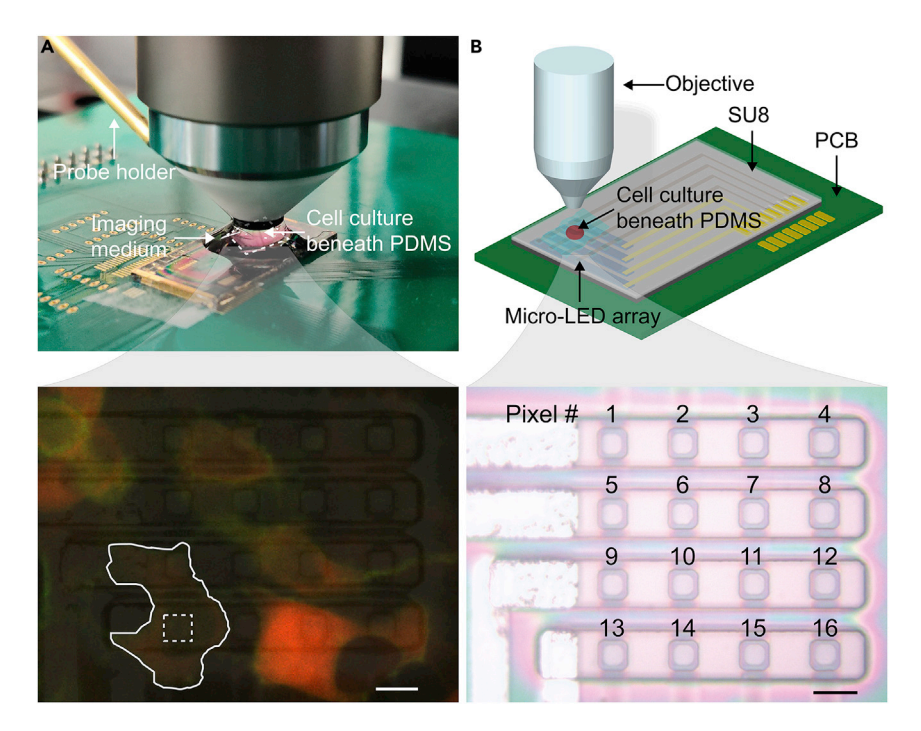


Figure 1. Experimental Setup

(A) One micro-LED array wired bonded onto a printed circuit board (PCB) under an upright fluorescence microscope configured for cell imaging. A flipped PDMS piece, seeded with cells on its top surface, was aligned to LED pixels by a probe holder; this way ChR2 (green)-jRCaMP1a (red) co-expressed cell (outlined) spatially overlapped with the LED pixel (squared). Scale bar, 10 µm.

(B) Illustration of the experimental setup using a 4-by-4 micro-LED array. Scale bar, 10 μm . See also Figures S1–S4.

signals among cells but also associate with complex synaptic chemistry (Garris, 2010; Andrews, 2013). These chemistries correlate with each other, play key roles in regulating cell activity, and add to high-content analysis of cell signaling. For instance, intracellular calcium concentration (i.e., [Ca²⁺]) is an essential biochemical signal in the regulation of muscle contraction, neurotransmitter release, and gene expression (Berridge et al., 2003; Clapham, 2007; Tu et al., 2016; Grewe et al., 2010; Seta et al., 2004).

To this end, here we demonstrate precise optogenetic control of intracellular Ca^{2+} dynamics at the single cell level using a 100%-yield, 16- μ m pitched micro-LED array that can output bright, localized, and fast-switching light in low-voltage operation. Single LED pixels are able to reliably trigger intracellular Ca^{2+} transients, evidenced by fluorescence microscopy, control groups, and comparative studies using two complementary Ca^{2+} indicators. Importantly, our array can optogenetically address individual cells that are sub-10 μ m apart in densely packed cell populations. Our results suggest the promise of the high-density micro-LED array toward a lab-on-a-chip for single-cell optogenetics. Combined with its highly scalable structure, this device may enable exciting opportunities in pharmaceutical screening and cell signaling studies in a variety of cell networks.

RESULTS

To conduct Ca²⁺ imaging under optogenetic stimulus, the activation spectrum of the optogenetic actuator and the excitation spectrum of the Ca²⁺ indicator need to be well separated from each other. This way we can minimize the optical cross talk between the excitation light (used for Ca²⁺ imaging) and the activation light (used for optogenetic control). Therefore, we selected two genetically coded Ca²⁺ indicators, *jRCaMP1a* and *NIR-GECO1* (Dana et al., 2016; Qian et al., 2019), each paired with an optogenetic actuator, *ChR2* (Zhang et al., 2007), and co-expressed them (either ChR2 with *jRCaMP1a* or ChR2 with *NIR-GECO1*) in HEK 293 cells seeded on a polydimethylsiloxane (PDMS) piece (Figures 1A and S1). We note that *NIR-GECO1* is an inverse response indicator to [Ca²⁺] change, which is opposite to *jRCaMP1a*. Therefore, a comparative study using these two complementary Ca²⁺ indicators can cross-check the effectiveness of the optogenetic stimulus applied in the cell experiment.



On the hardware side, we fabricated a GaN-based, 4-by-4 micro-LED array that can output 462/19 nm light to activate ChR2 (Figure S2). This device was built on commercial epitaxial GaN-on-Si wafers, formed by sequentially growing multiple GaN-based layers on top of a (111) Si substrate (see Figure S3 and Transparent Methods). Using reactive-ion etching steps, a total of 16 LED pixels, each 6.5 μ m-by-6.5 μ m in size, were patterned in a cross-bar structure with a 16- μ m pitch (Figure 1B). We noted that this pitch size is three times smaller than previous GaN-based LED arrays used for optogenetics (Poher et al., 2008; Grossman et al., 2010; McGovern et al., 2010) and close to the typical diameter of a HEK 293 cell. The column and row select lines of the array were formed by Ni/indium tin oxide (5/120 nm for p-GaN contacts) and Ti/Al/Ti/Au layers (10/70/10/120 nm for n-GaN contacts), respectively, and passivated by plasma-enhanced chemical vapor deposition-based SiO₂ (PECVD- SiO₂) layers. The array was then encapsulated by another PECVD-SiO₂ layer (~200 nm) with a cross-linked SU8 layer on top and wire-bonded onto a printed circuit board for pixel selection (Figure S4). During cell experiments, we flipped a PDMS piece seeded with cells and placed it onto the encapsulated array (Figure 1B). This way, cells faced the LED pixels and could be aligned to the pixel of interest by moving the PDMS piece with a micro-manipulator (see the probe holder in Figure 1A).

To enable optogenetic control at the single cell level, the micro-LED array is required to output bright, localized, and fast-switching light, ideally in a low-voltage operation. To this end, we first measured the optical power density (P_{light}) and the spatial profile of the illumination spot (I_{light}) of each LED pixel, using an optical power meter and a fluorescence microscope, respectively. When biased at injection currents (I_{LED}) ranging from 0.1 to 2.0 μ A, all 16 pixels show high brightness with $P_{\text{light}} \sim 0.1-1.0 \,\text{mW/mm}^2$ (Figure 2A), which falls into the range required for optogenetic control in HEK 293 cells and mammalian neurons (Boyden et al., 2005; Steude et al., 2016; Morton et al., 2019). We note that this high brightness is achieved with the driving voltage across each pixel (V_{LED}) being less than 4.8 V (Figure 2B). This low-voltage operation leads to sub-10-μW electrical power dissipation per pixel, which may ultimately allow for in vivo use (Marblestone et al., 2013; Mao et al., 2018). Moreover, at $I_{LED} = 1.0$ or $1.5 \,\mu\text{A}$, all 16 pixels output small light spots with the full width at half maximum (FWHM) $< 10 \, \mu m$ at the array surface (Figures 2C and 2D, the FWHM is overestimated here as the center of the light spot in some pixels saturates the camera). Importantly, this localized pixel output with $P_{\text{light}} \sim 0.5$ –0.8 mW/mm 2 is encouraging for optogenetic control over single cells close to the array surface, as HEK 293 cells are \sim 10 μ m in size. Finally, we found that such bright, localized pixel output (i.e., $P_{\text{light}} \sim 0.5 \text{ mW/mm}^2$, FWHM <10 μ m) can be pulsed with a 10-ms duration at up to 40-Hz pulsing frequencies (Figure 2E). After 3 ms in each pulse, the pulsed light intensity approached to its steady state value, with <3% variation among all pulses during 1-s recording. These results suggest that our LEDs meet the brightness, resolution, and speed requirement for optogenetic studies at cellular levels.

To prepare the optogenetic experiments, we flipped the PDMS piece—seeded with HEK 293 cells on its top surface—and placed it onto the array to let cells face the LED pixels. This PDMS-flipping approach adds to single-cell optogenetics in two ways. First, by getting cells closer to the array, this approach enhances the amount of light each cell receives and thus the strength of optogenetic control. Second, since LEDs emit light omnidirectionally, the spatial resolution they can offer is better close to the array surface, where the light spot is smaller. On the biology side, we cultured HEK 293 cells on sterilized PDMS pieces at 37°C in a humidified incubator, added the co-factor *all-trans retinal* to enhance light transduction of *ChR2* (Steude et al., 2016; Cho et al., 2019), and transfected one of the two Ca²⁺ indicators with (co-transfection) or without (single transfection) *ChR2* into these cells, all following the manufacturers' recommended protocols (see Transparent Methods). Before optogenetic experiments, we added an imaging solution containing 80 mM CaCl₂ to cell culture, which serves to enhance cell responses to optogenetic stimulus as more extracellular Ca²⁺ would flush into the cell when *ChR2* gets activated (Cho et al., 2019; Lin et al., 2009).

With these preparation steps, we next conducted optogenetic experiments using a standard Ca^{2+} imaging configuration by a fluorescence microscope. During each experiment, we pulsed 575/25-nm excitation light using the microscope with 0.5 frame per second and 100-ms exposure time per frame to alleviate the photo-bleaching effect. Meanwhile, the cell of interest was optogenetically stimulated by LED pixels in three consecutive recording periods. In each period, we illuminated the select LED pixel 20 s after the Ca^{2+} signal of the cell reached the steady state, with the excitation light being shut off at the same time. Here we chose not to collect Ca^{2+} imaging data during the optogenetic stimulation since the LED light would otherwise leak through the emission filter, introduce an artifact in the Ca^{2+} imaging data, and obscure the analysis. In parallel, we also conducted experiments with the optogenetic stimulus being

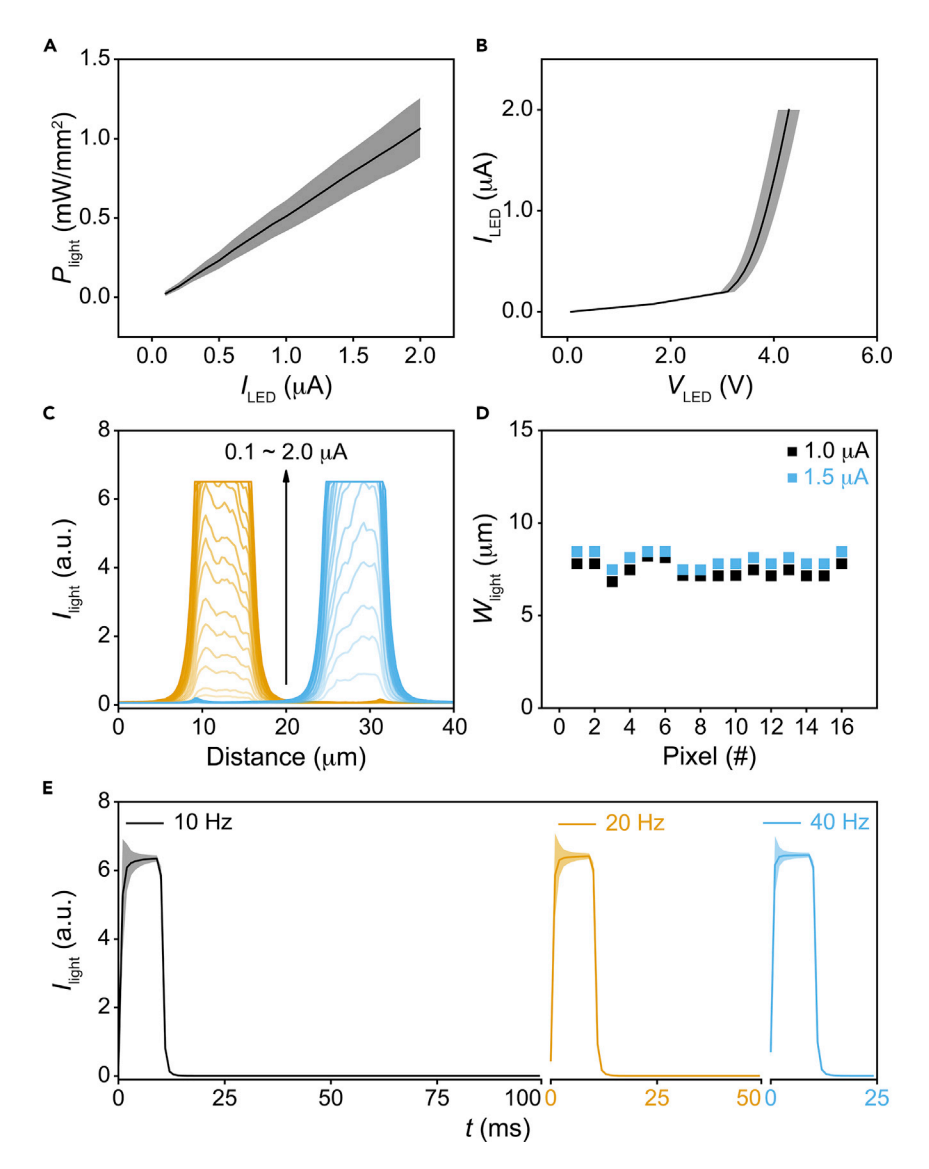


Figure 2. Array Characterization

- (A) P_{light} versus I_{LED} for all 16 pixels.
- (B) I_{LED} - V_{LED} curves for all 16 pixels.
- (C) Spatial profile of the pixel output (from two neighboring pixels) at the array surface with I_{LED} ranging from 0.1 to 2.0 μ A. (D) FWHM values of all 16 pixels with I_{LED} = 1.0 and 1.5 μ A.
- (E) Pixel output pulsed with a 10-ms pulse duration at 10- to 40-Hz pulsing frequencies. The pixel was biased at $I_{LED} = 2.0 \,\mu$ A. In (A), (B), and (E), shaded areas represent $\pm 1 \, \text{SD}$.

provided by the microscope (3.92 mW at 470/24 nm), in which case all cells in the field of view were illuminated simultaneously.

After each optogenetic stimulation with I_{LED} ranging from 0.5 to 1.5 μ A and the duration (T_{LED}) ranging from 10 to 40 s, ChR2-jRCaMP1a co-expressed cells were found to reliably increase their emitted fluorescence intensities (Figures 3A and 3B). Here we define the F_0 value as the 20-s average before each stimulation, subtracted by the background measured at the dark region in the field of view. The resulting positive $\Delta F/F_0$ values after each stimulation suggest an increase of intracellular Ca^{2+} level, coming from the optogenetically triggered Ca^{2+} influx to the illuminated cell (Dana et al., 2016; Morton et al., 2019). To examine if such Ca^{2+} increase was specific to the optogenetic activation of ChR2, we conducted control experiments with cells that are transfected with jRCaMP1a only (i.e., control cells). Indeed, these cells did not increase

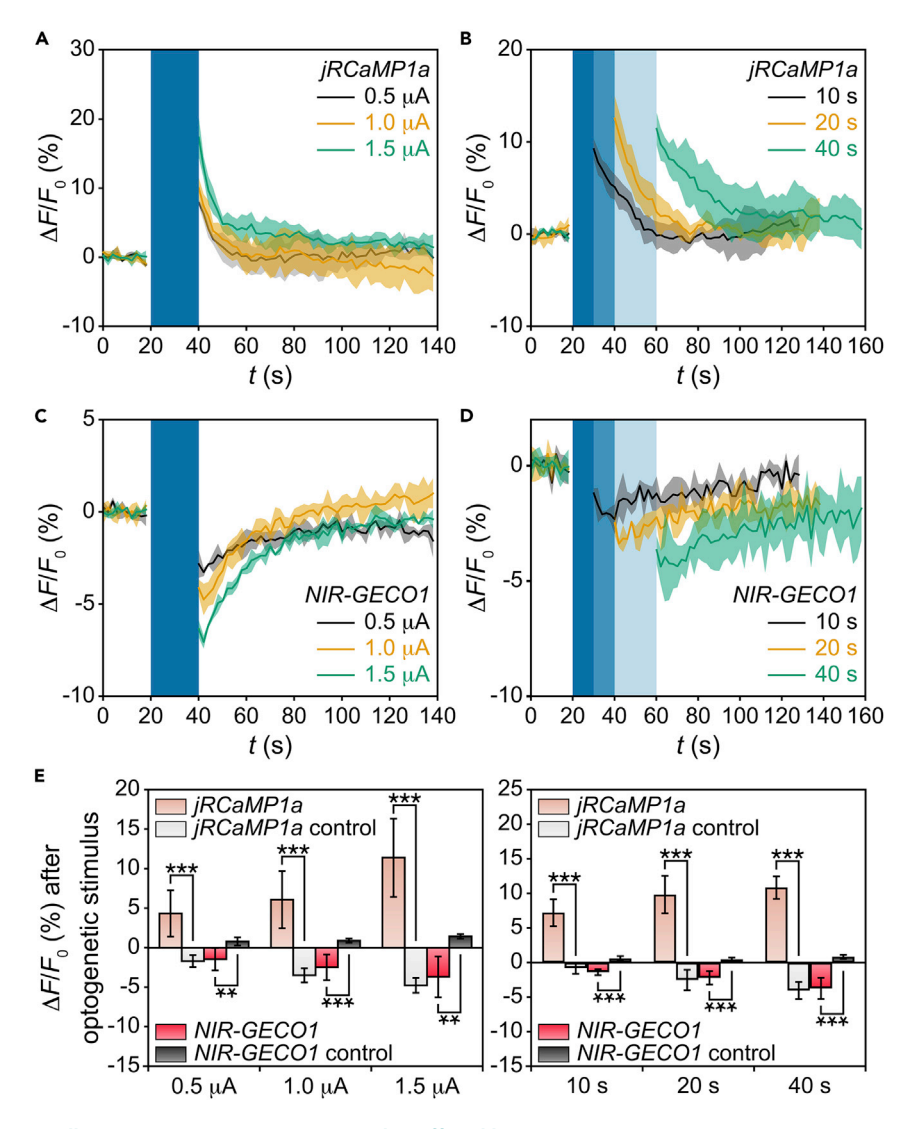


Figure 3. Cell Responses to Optogenetic Stimulus Offered by LEDs

(A) $\Delta F/F_0$ traces from a ChR2-jRCaMP1a co-expressed cell with $T_{LED}=20$ s and I_{LED} ranging from 0.5 to 1.5 μ A. (B) $\Delta F/F_0$ traces from a ChR2-jRCaMP1a co-expressed cell with T_{LED} ranging from 10 to 40 s and I_{LED} = 1.5 μ A. (C) $\Delta F/F_0$ traces from a ChR2-NIR-GECO1 co-expressed cell with $T_{LED} = 20$ s and I_{LED} ranging from 0.5 to 1.5 μ A. (D) Representative $\Delta F/F_0$ traces from a ChR2-NIR-GECO1 co-expressed cell with T_{LED} ranging from 10 to 40 s and I_{LED} = $1.5 \,\mu\text{A}$. In (A), (B), (C), and (D), blue windows represent the periods of optogenetic stimulus; solid lines represent the mean values from three consecutive recording periods; shaded areas represent ± 1 SD.

(E) $\Delta F/F_0$ signals versus I_{LED} (left) and T_{LED} (right) in both co-expressed and control cells. Error bars represent ± 1 SD (n=9) from three independent cells in each group, three recording periods from each cell); **p < 0.01, ***p < 0.001 based on Student's t test.

See also Figures S5 and S6.

their $\Delta F/F_0$ values after optogenetic stimulus since no ChR2 were expressed to assist the Ca²⁺ influx (Figure S5). We confirmed these results by additional experiments with cells being optogenetically stimulated by the microscope (i.e., microscope-based stimulus), which yielded qualitatively similar $\Delta F/F_0$ traces in both co-expressed and control cells (Figure S6).

On the other hand, we found that ChR2-NIR-GECO1 co-expressed cells reliably decreased their emitted fluorescence intensities by optogenetic stimulus (Figures 3C and 3D). The resulting negative $\Delta F/F_0$ values are opposite to that in ChR2-jRCaMP1a co-expressed cells, because NIR-GECO1 is an inverse response indicator to the optogenetically triggered Ca²⁺ influx (Qian et al., 2019). In the control experiments, cells only



transfected with NIR-GECO1 did not decrease $\Delta F/F_0$ values after optogenetic stimulus since no ChR2 were expressed to assist the Ca²⁺ influx (Figure S5). Likewise, we confirmed these results by additional experiments with microscope-based optogenetic stimulus, which yielded similar $\Delta F/F_0$ traces (Figure S6). These data with NIR-GECO1 being the Ca²⁺ indicator further validate the effectiveness of the optogenetic stimulus offered by LEDs.

To quantify the strength of the applied optogenetic stimulus, here we define the $\Delta F/F_0$ value right after each optogenetic stimulus as our signal. To perform statistical analysis, we collected data from three independent *ChR2-jRCaMP1a* co-expressed cells, *ChR2-NIR-GECO1* co-expressed cells, or their corresponding control cells. Since each cell was tested in three consecutive recording periods, our statistics is based on n = 9 such periods from three independent cells (Figure 3E).

In ChR2-jRCaMP1a co-expressed cells, the $\Delta F/F_0$ value after optogenetic stimulus is positive and mildly increases with $I_{\rm LED}$ and $T_{\rm LED}$. This dependence is likely because more LED stimulus, by increasing either $I_{\rm LED}$ or $T_{\rm LED}$, would increase the amount of ${\rm Ca^{2^{+}}}$ influx by opening more ChR2-related ${\rm Ca^{2^{+}}}$ channels. In contrast, among jRCaMP1a control cells, the $\Delta F/F_0$ value after optogenetic stimulus becomes negative (confirmed by additional experiments using microscope-based stimulus, see Figure S6) and mildly increases its amplitude (i.e., absolute value) with $I_{\rm LED}$ and $T_{\rm LED}$. This negative $\Delta F/F_0$ value in jRCaMP1a control cells is likely due to the temporary photobleaching of jRCaMP1a by the 10- to 40-s constant LED illumination, which was later recovered at the end of each recording period. Another possible reason is that such constant LED illumination may temporarily increase the local temperature (Marblestone et al., 2013) and thus decrease the local pH next to the cell of interest. This local pH decrease can temporarily lower the fluorescence intensity of jRCaMP1a as reported before (Oliver et al., 2000; Kerruth et al., 2019; Zhao et al., 2011).

On the other hand, in *ChR2-NIR-GECO1* co-expressed cells, the $\Delta F/F_0$ value after optogenetic stimulus is negative and mildly increases its amplitude (i.e., absolute value) with I_{LED} and T_{LED} . Again, this dependence is likely because the Ca²⁺ influx increases with the strength of the optogenetic stimulus offered by LEDs. In contrast, among *NIR-GECO1* control cells, the $\Delta F/F_0$ value after optogenetic stimulus is found to be positive (confirmed by additional experiments using microscope-based stimulus, see Figure S6) and slightly increases with I_{LED} and T_{LED} . This positive $\Delta F/F_0$ value in *NIR-GECO1* control cells is also likely because the 10- to 40-s constant LED illumination temporarily increased the local temperature and thus decreased the local pH next to the cell of interest. Such pH decrease (\sim 7.3 in the imaging solution) can temporarily enhance the fluorescence intensity of *NIR-GECO1* as reported before (Qian et al., 2019). Another possibility is that such constant LED illumination may get *NIR-GECO1* photoisomerized to a metastable brighter state, which was later overwhelmed by the photobleaching effect at the end of each recording period.

In comparison, we found that ChR2-jRCaMP1a co-expressed cells were overall brighter and had larger $\Delta F/F_0$ signals. ChR2-NIR-GECO1 co-expressed cells were overall inferior in these two aspects, but provided robust reverse response to Ca^{2+} changes, and helped cross-check if the optogenetic stimulus offered by LEDs was effective. In addition, our LEDs can typically generate $\Delta F/F_0$ values that are on par with—if not larger than—those generated by microscope-based stimulus (Figure S6). This fact re-affirms that our LEDs can indeed provide reliable optogenetic control of Ca^{2+} signaling.

After validating the performance of our micro-LEDs, we now examine if they can provide precise optogenetic control at the single cell level in dense cell populations. To achieve this, we chose to optogenetically stimulate one pair of neighboring ChR2-jRCaMP1a co-expressed cells using different LED pixels (Figure 4), all with $T_{\text{LED}} = 20 \, \text{s}$ and $P_{\text{light}} \sim 0.71 \, \text{mW/mm}^2$ to compare their evoked $\Delta F/F_0$ signals (note: different pixels were biased at different I_{LED} owing to pixel-to-pixel variation).

Specifically, cell 1 (overlapped with pixel 13) and cell 2 (overlapped with pixel 8) were sub-10 μ m apart with an ~50 μ m center-to-center distance (Figure 4A). Our data in Figures 4B–4D show that (1) cell 1 had significantly larger $\Delta F/F_0$ signals when it got stimulated by pixel 13 than when it got stimulated by pixel 8 and (2) cell 2 had significantly larger $\Delta F/F_0$ signals when it got stimulated by pixels 8 than when it got stimulated by pixel 13. These results show that *ChR2*-expressed cells indeed responded more to LED pixels that were overlapped with them. Moreover, *either* pixel 8 *or* pixel 13 introduced low cross talk in the cell that was not overlapped with the pixel; the $\Delta F/F_0$ signal in the cell that was overlapped with the pixel

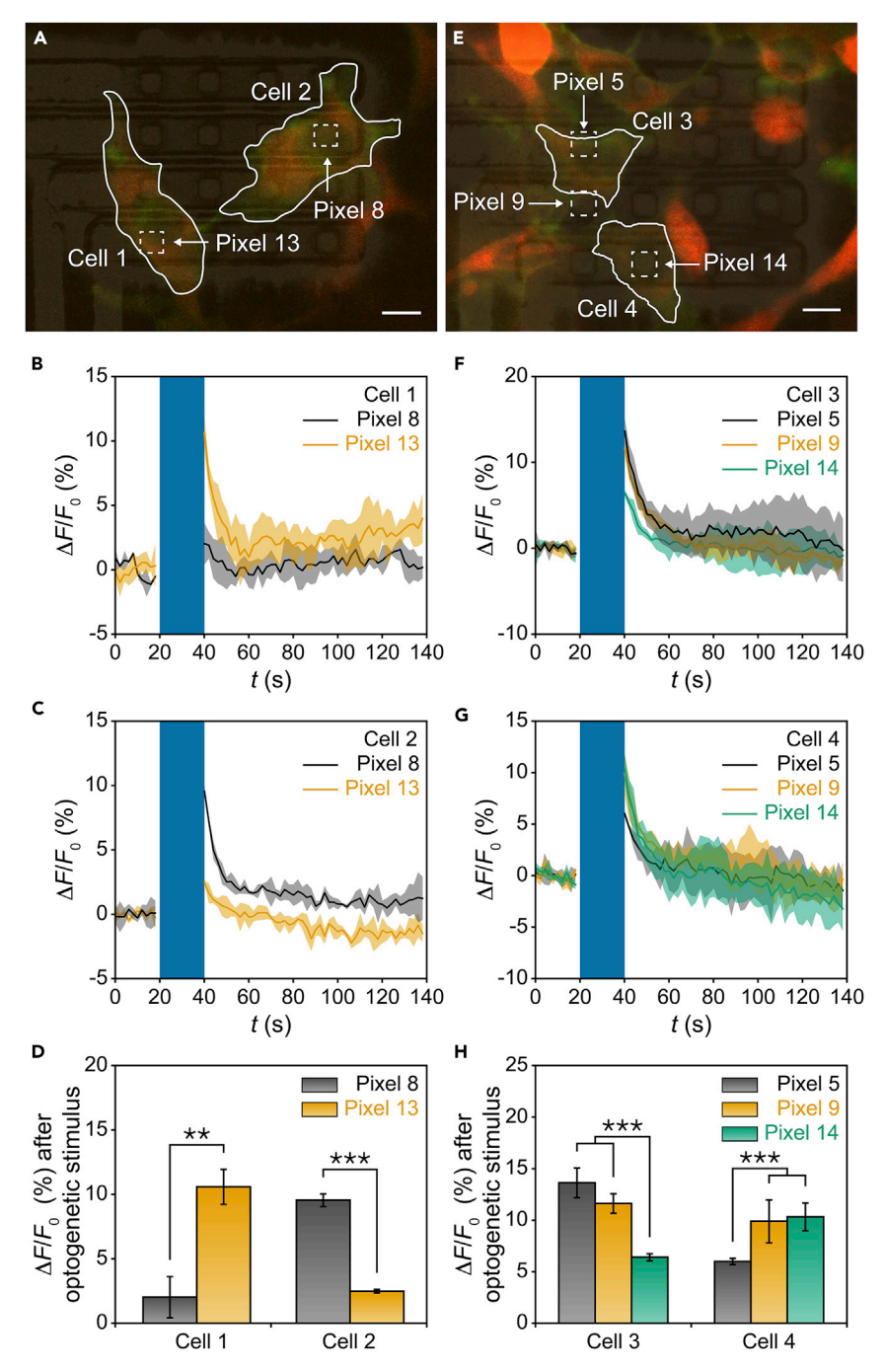


Figure 4. Spatial Resolution of the Optogenetic Stimulus Offered by LEDs

- (A) One pair of cells (outlined, overlapped with pixels 13 and 8) that were sub-10 μm apart. Scale bar, 10 μm .
- (B) $\Delta F/F_0$ traces of cell 1 stimulated by pixels 8 and 13 with $T_{LED} = 20$ s.
- (C) $\Delta F/F_0$ traces of cell 2 stimulated by pixels 8 and 13 with $T_{\rm LED}$ = 20 s.
- (D) Statistical analysis of $\Delta F/F_0$ signals from cell 1 and cell 2.
- (E) Another pair of cells (outlined, overlapped with pixels 5, 9, and 14) that were sub-5 μ m apart. Scale bar, 10 μ m.
- (F) $\Delta F/F_0$ traces of cell 3 stimulated by pixels 5, 9, and 14 with T_{LED} = 20 s.
- (G) $\Delta F/F_0$ traces of cell 4 stimulated by pixels 5, 9, and 14 with $T_{LED} = 20$ s.
- (H) Statistical analysis of $\Delta F/F_0$ signals from cell 3 and cell 4.



Figure 4. Continued

In (B), (C), (F), and (G), blue windows represent the periods of optogenetic stimulus; solid lines represent the mean values from three consecutive recording periods; shaded areas represent ± 1 SD. The I_{LED} values applied to output $P_{light} \sim 0.71 \, \text{mW/mm}^2$ were $1.2 \, \mu\text{A}$ for pixel 5, $1.6 \, \mu\text{A}$ for pixel 8, $1.5 \, \mu\text{A}$ for pixel 9, $1.0 \, \mu\text{A}$ for pixel 13, and $1.1 \, \mu\text{A}$ for pixel 14. In (D) and (H), error bars represent $\pm 1 \, \text{SD}$ (n=3 recording periods); **p < 0.01, ***p < 0.001 based on Student's t test. See also Figure S7.

than three times that in the cell that was not overlapped with the pixel (i.e., selectivity >3). Importantly, these data suggest that our array can indeed address individual cells that are sub-10 μ m apart with low cross talk; pixels 13 and 8 can provide such precise optogenetic control over cell 1 and cell 2, respectively.

To examine the limit of spatial resolution our array can achieve, we conducted another experiment (Figure 4E) with two cells even closer to each other. Specifically, cell 3 (overlapped with pixels 5 and 9) and cell 4 (overlapped with pixel 14, spatially closer to pixel 9 than pixel 5) were sub-5 μ m apart with an ~30- μ m center-to-center distance. Our data in Figures 4F–4H show that (1) cell 3 had significantly larger $\Delta F/F_0$ signals when it got stimulated by pixels 5 and 9 than when it got stimulated by pixel 14 and (2) cell 4 had significantly larger $\Delta F/F_0$ signals when it got stimulated by pixels 14 and 9 than when it got stimulated by pixel 5. These results reaffirm that ChR2-expressed cells responded more to LED pixels that were overlapped with or closer to them. The fact that cell 4 responded similarly to pixels 9 and 14 is likely because cell 4 was far away from the array surface, where the pixel 9 output was less confined (i.e., spot size increased to >10 μ m). However, it is noted that the selectivity in this experiment was less than 3, suggesting that our array cannot address individual cells that are sub-5 μ m apart with low cross talk. Taking one step further, we observed that the selectivity was even lower (consistently <2) when cells were sub-1 μ m apart (see additional two experiments in Figure S7). We thus conclude that our array can currently achieve sub-10- μ m resolution.

DISCUSSION

In sum, we demonstrated optogenetic control of Ca^{2+} signaling at the single-cell level using a 100%-yield high-density micro-LED array. Our array was found to output bright, localized, and fast-switching light in a low-voltage operation, which can precisely address individual HEK 293 cells that were sub-10 μ m apart. Importantly, our results were confirmed by epifluorescence microscopy, control experiments, and cross-checked by two complementary Ca^{2+} indicators, all of which showed statistical significance. This work suggests the promise of the high-density micro-LED array toward a lab-on-a-chip for single-cell optogenetics, which can add to high-content cell signaling studies. Combined with its highly scalable structure, this device may provide a cost-effective platform for pharmaceutical screening and fundamental studies on a variety of cell networks. Leveraging standard semiconductor fabrication steps, our LED arrays can, for instance, readily extend to a medium number of pixels (\sim 100) to study computational algorithms of the neural network at the *in vitro* setting. On the other hand, we can create alternative versions of the array to output different wavelengths in the visible spectrum. For example, AlGalnP-based micro-LED arrays can be similarly built to output 600–630 nm light, which can be applied to actuate red-shifted opsins (e.g., *Chrimson*) and monitor intracellular Ca^{2+} dynamics using green Ca^{2+} indicators (e.g., *GCaMP7*) at the same time (Klapoetke et al., 2014; Dana et al., 2019).

Finally, we remark that our high-performance array can be used to study single-cell optogenetics in other cell types (e.g., neurons or cardiomyocytes) and provide precise optogenetic control over other cellular signals (e.g., intracellular potassium concentration). For *ex-vivo* or *in vivo* applications our arrays will need to be encapsulated by biocompatible and transparent films (e.g., SU8 or epoxy). Furthermore, if built along a solid-state shank similar to that of the implantable silicon microelectrode arrays (Scholvin et al., 2016), the resulting device would be typically sub-100 μ m wide, sub-100 μ m thick, and 3–5 mm long, which may ultimately enable single-cell optogenetics in deep tissues. By sequentially illuminating individual pixels, such device would routinely consume sub-10 mW electrical power, which is suitable for long term *in vivo* use. If successful, for instance, one may implant such devices to trigger intracellular [Ca²⁺] change during muscle recovery from injury (van Bremen et al., 2017) or to offer precise modulation of the neurocircuitry in deep brain (Yawo et al., 2013).

Limitations of the Study

The energy conversion efficiency of our LED pixels, defined as the value of $P_{\text{light}}/(I_{\text{LED}} \cdot V_{\text{LED}})$ here, suffered from voltage drop across the contact wires. To solve this issue, our array layout will need to be further



optimized to reduce the series resistance from these contact wires. On the other hand, we may be able to change the constant LED illuminations to pulsed LED illuminations. We expect such change would alleviate the local heating effect to the cell of interest. Furthermore, by alternatingly pulsing LED illuminations and the excitation light (i.e., not turning them on at the same time), we might be able to monitor intracellular Ca²⁺ dynamics during the period of optogenetic stimulus; we did not do this with constant LED illuminations in this work, because the bright LED output was found to partially leak through the emission filters of the microscope and act as the background noise for Ca²⁺ imaging. In terms of the biocompatibility, our LEDs passivated with an SU8 layer were able to monitor cell activity for ca. 1.5 h at room temperature. We expect that this period can be further extended if cells on the array could be kept at ~37°C by a fixed heating stage. Last but not least, the spatial resolution of our array is currently limited by the omnidirectional emission from LEDs and can be improved by adding light guide or microlens layers in the future.

METHODS

All methods can be found in the accompanying Transparent Methods supplemental file.

DATA AND CODE AVAILABILITY

All data generated or analyzed during this study are included in this published article and its Supplemental Information.

SUPPLEMENTAL INFORMATION

Supplemental Information can be found online at https://doi.org/10.1016/j.isci.2019.10.024.

ACKNOWLEDGMENTS

This work was supported by the National Science Foundation under ECCS-1835268 and CMMI-1662835. The authors thank A. Arbabi, Y. Zhao, K. D. Piatkevich, T. Xie, and H. Tan for scientific discussions and technical assistance.

AUTHOR CONTRIBUTIONS

G.X. conceived and supervised the project. D.M. designed, fabricated, and characterized the arrays. N.L., D.M., and Y.S. prepared cell culture and developed the protocols for cell experiments. D.M. and Z.X. performed the cell experiments. Z.X., D.M., and G.X. analyzed the data and wrote the paper. All authors discussed the results and reviewed the manuscript.

DECLARATION OF INTERESTS

The authors declare no competing interests.

Received: August 9, 2019 Revised: October 8, 2019 Accepted: October 11, 2019 Published: November 22, 2019

REFERENCES

Abbott, J., Ye, T., Qin, L., Jorgolli, M., Gertner, R.S., Ham, D., and Park, H. (2017). CMOS nanoelectrode array for all-electrical intracellular electrophysiological imaging. Nat. Nanotechnol. 12, 460–466.

Andrews, A.M. (2013). The BRAIN initiative: toward a chemical connectome. ACS Chem. Neurosci, 4, 645.

Asano, T., Ishizuka, T., Morishima, K., and Yawo, H. (2015). Optogenetic induction of contractile ability in immature C2C12 myotubes. Sci. Rep. 5, 8317.

Baaske, J., Gonschorek, P., Engesser, R., Dominguez-Monedero, A., Raute, K., Fischbach, P., Müller, K., Cachat, E., Schamel, W.W., Minguet, S., et al. (2018). Dual-controlled optogenetic system for the rapid downregulation of protein levels in mammalian cells. Sci. Rep. 8, 15024.

Berridge, M.J., Bootman, M.D., and Roderick, H.L. (2003). Calcium signalling: dynamics, homeostasis and remodelling. Nat. Rev. Mol. Cell Biol. 4, 517-529.

Boyden, E.S. (2015). Optogenetics and the future of neuroscience. Nat. Neurosci. 18, 1200-1201.

Boyden, E.S., Zhang, F., Bamberg, E., Nagel, G., and Deisseroth, K. (2005). Millisecond-timescale, genetically targeted optical control of neural activity. Nat. Neurosci. 8, 1263-1268.

Cho, Y.K., Park, D., Yang, A., Chen, F., Chuong, A.S., Klapoetke, N.C., and Boyden, E.S. (2019). Multidimensional screening yields channelrhodopsin variants having improved photocurrent and order-of-magnitude reductions in calcium and proton currents. J. Biol. Chem. 294, 3806-3821.

Chow, B.Y., Han, X., Dobry, A.S., Qian, X., Chuong, A.S., Li, M., Henninger, M.A., Belfort,



G.M., Lin, Y., Monahan, P.E., et al. (2010). Highperformance genetically targetable optical neural silencing by light-driven proton pumps. Nature 463, 98-102.

Clapham, D.E. (2007). Calcium signaling. Cell 131, 1047-1058.

Dana, H., Mohar, B., Sun, Y., Narayan, S., Gordus, A., Hasseman, J.P., Tsegaye, G., Holt, G.T., Hu, A., Walpita, D., et al. (2016). Sensitive red protein calcium indicators for imaging neural activity. Elife 5, e12727.

Dana, H., Sun, Y., Mohar, B., Hulse, B.K., Kerlin, A.M., Hasseman, J.P., Tsegaye, G., Tsang, A., Wong, A., Patel, R., et al. (2019). Highperformance calcium sensors for imaging activity in neuronal populations and microcompartments. Nat. Methods 16, 649-657.

Deisseroth, K. (2015). Optogenetics: 10 years of microbial opsins in neuroscience. Nat. Neurosci. 18, 1213–1225.

Garris, P.A. (2010). Advancing neurochemical monitoring. Nat. Methods 7, 106-108.

Grewe, B.F., Langer, D., Kasper, H., Kampa, B.M., and Helmchen, F. (2010). High-speed in vivo calcium imaging reveals neuronal network activity with near-millisecond precision. Nat. Methods 7 399-405.

Grossman, N., Poher, V., Grubb, M.S., Kennedy, G.T., Nikolic, K., McGovern, B., Palmini, R.B., Gong, Z., Drakakis, E.M., Neil, M.A., et al. (2010). Multi-site optical excitation using ChR2 and micro-LED array. J. Neural Eng. 7, 016004.

Hierlemann, A., Frey, U., Hafizovic, S., and Heer, F. (2011). Growing cells atop microelectronic chips: interfacing electrogenic cells in vitro with CMOS-based microelectrode arrays. Proc. IEEE 99, 252-284.

Hochbaum, D.R., Zhao, Y., Farhi, S.L., Klapoetke, N., Werley, C.A., Kapoor, V., Zou, P., Kralj, J.M., Maclaurin, D., Smedemark-Margulies, N., et al. (2014). All-optical electrophysiology in mammalian neurons using engineered microbial rhodopsins. Nat. Methods 11, 825-833.

Johnston, C.M., Rog-Zielinska, E.A., Wülfers, E.M., Houwaart, T., Siedlecka, U., Naumann, A., Nitschke, R., Knöpfel, T., Kohl, P., and Schneider-Warme, F. (2017). Optogenetic targeting of cardiac myocytes and non-myocytes: tools, challenges and utility. Prog. Biophys. Mol. Biol. 130, 14Ō-149.

Kerruth, S., Coates, C., Dürst, C.D., Oertner, T.G., and Török, K. (2019). The kinetic mechanisms of fast-decay red-fluorescent genetically encoded calcium indicators. J. Biol. Chem. 294, 3934-3946.

Klapoetke, N.C., Murata, Y., Kim, S.S., Pulver, S.R., Birdsey-Benson, A., Cho, Y.K., Morimoto, T.K., Chuong, A.S., Carpenter, E.J., Tian, Z., et al. (2014). Independent optical excitation of distinct neural populations. Nat. Methods 11, 338-346.

Lin, J.Y., Lin, M.Z., Steinbach, P., and Tsien, R.Y. (2009). Characterization of engineered channelrhodopsin variants with improved properties and kinetics. Biophys. J. 96, 1803-

Lu, Y., Liu, X., and Kuzum, D. (2018). Graphenebased neurotechnologies for advanced neural interfaces. Curr. Opin. Biomed. Eng. 6, 138-147.

Mao, D., Morley, J., Zhang, Z., Donnelly, M., and Xu, G. (2018). High-yield passive Si photodiode array towards optical neural recording. IEEE Electron Device Lett. 39, 524-527.

Marblestone, A.H., Zamft, B.M., Maguire, Y.G., Shapiro, M.G., Cybulski, T.R., Glaser, J.I. Amodei, D., Stranges, P.B., Kalhor, R., Dalrymple, D.A., et al. (2013). Physical principles for scalable neural recording. Front. Comput. Neurosci. 7,

McGovern, B., Palmini, R.B., Grossman, N., Drakakis, E.M., Poher, V., Neil, M.A.A., and Degenaar, P. (2010). A new individually addressable micro-LED array for photogenetic neural stimulation. IEEE Trans. Biomed. Circuits Syst. 4, 469-476.

Miyazaki, T., Chowdhury, S., Yamashita, T., Matsubara, T., Yawo, H., Yuasa, H., and Yamanaka, A. (2019). Large timescale interrogation of neuronal function by fiberless optogenetics using lanthanide micro-particles. Cell Rep. 26, 1033-1043.

Morton, A., Murawski, C., Deng, Y., Keum, C. Miles, G.B., Tello, J.A., and Gather, M.C. (2019). Photostimulation for in vitro optogenetics with high-power blue organic light-emitting diodes. Adv. Biosyst. 3, 1800290.

Nakajima, A., Kimura, H., Sawadsaringkarn, Y., Maezawa, Y., Kobayashi, T., Noda, T., Sasagawa, K., Tokuda, T., Ishikawa, Y., Shiosaka, S., et al. (2012). CMOS image sensor integrated with micro-LED and multielectrode arrays for the patterned photostimulation and multichannel recording of neuronal tissue. Opt. Express 20, 6097-6108.

Oliver, A.E., Baker, G.A., Fugate, R.D., Tablin, F., and Crowe, J.H. (2000). Effects of temperature on calcium-sensitive fluorescent probes. Biophys. J. 78, 2116–2126.

Pisanello, F., Sileo, L., and De Vittorio, M. (2016). Micro-and nanotechnologies for optical neural interfaces. Front. Neurosci. 10, 70.

Poher, V., Grossman, N., Kennedy, G.T., Nikolic, K., Zhang, H.X., Gong, Z., Drakakis, E.M., Gu, E., Dawson, M.D., French, P.M.W., et al. (2008). Micro-LED arrays: a tool for two-dimensional neuron stimulation. J. Phys. D Appl. Phys. 41,

Prakash, R., Yizhar, O., Grewe, B., Ramakrishnan, C., Wang, N., Goshen, I., Packer, A.M., Peterka, D.S., Yuste, R., Schnitzer, M.J., et al. (2012). Twophoton optogenetic toolbox for fast inhibition,

excitation and bistable modulation. Nat. Methods 9, 1171-1179.

Qian, Y., Piatkevich, K.D., Mc Larney, B., Abdelfattah, A.S., Mehta, S., Murdock, M.H., Gottschalk, S., Molina, R.S., Zhang, W., Chen, Y., et al. (2019). A genetically encoded near-infrared fluorescent calcium ion indicator. Nat. Methods 16, 171-174.

Scholvin, J., Kinney, J.P., Bernstein, J.G., Moore-Kochlacs, C., Kopell, N., Fonstad, C.G., and Boyden, E.S. (2016). Close-packed silicon microelectrodes for scalable spatially oversampled neural recording. IEEE Trans. Biomed. Eng. 63, 120–130.

Sebille, S., Ayad, O., Chapotte-Baldacci, C.A., Cognard, C., Bois, P., and Chatelier, A. (2017). Optogenetic approach for targeted activation of global calcium transients in differentiated C2C12 myotubes. Sci. Rep. 7, 11108.

Seta, K.A., Yuan, Y., Spicer, Z., Lu, G., Bedard, J., Ferguson, T.K., Pathrose, P., Cole-Strauss, A., Kaufhold, A., and Millhorn, D.E. (2004). The role of calcium in hypoxia-induced signal transduction and gene expression. Cell Calcium 36, 331-340.

Steude, A., Witts, E.C., Miles, G.B., and Gather, M.C. (2016). Arrays of microscopic organic LEDs for high-resolution optogenetics. Sci. Adv. 2, e1600061.

Tu, M.K., Levin, J.B., Hamilton, A.M., and Borodinsky, L.N. (2016). Calcium signaling in skeletal muscle development, maintenance and regeneration. Cell Calcium 59, 91-97.

van Bremen, T., Send, T., Sasse, P., and Bruegmann, T. (2017). Spot light on skeletal muscles: optogenetic stimulation to understand and restore skeletal muscle function. J. Muscle Res. Cell. Motil. 38, 331-337.

Wang, Y., Lin, W.K., Crawford, W., Ni, H., Bolton, E.L., Khan, H., Shanks, J., Bub, G., Wang, X., Paterson, D.J., et al. (2017). Optogenetic control of heart rhythm by selective stimulation of cardiomyocytes derived from Pnmt+ cells in murine heart. Sci. Rep. 7, 40687.

Yawo, H., Asano, T., Sakai, S., and Ishizuka, T. (2013). Optogenetic manipulation of neural and non-neural functions. Dev. Growth Differ. 55, 474-490.

Zhang, F., Wang, L.P., Brauner, M., Liewald, J.F., Kay, K., Watzke, N., Wood, P.G., Bamberg, E., Nagel, G., Gottschalk, A., et al. (2007). Multimodal fast optical interrogation of neural circuitry. Nature 446, 633-639.

Zhao, Y., Araki, S., Wu, J., Teramoto, T., Chang, Y.F., Nakano, M., Abdelfattah, A.S., Fujiwara, M., Ishihara, T., Nagai, T., et al. (2011). An expanded palette of genetically encoded Ca2+ indicators. Science 333, 1888–1891.

Supplemental Information

Single-Cell Optogenetic Control of Calcium
Signaling with a High-Density Micro-LED Array

Dacheng Mao, Ningwei Li, Zheshun Xiong, Yubing Sun, and Guangyu Xu

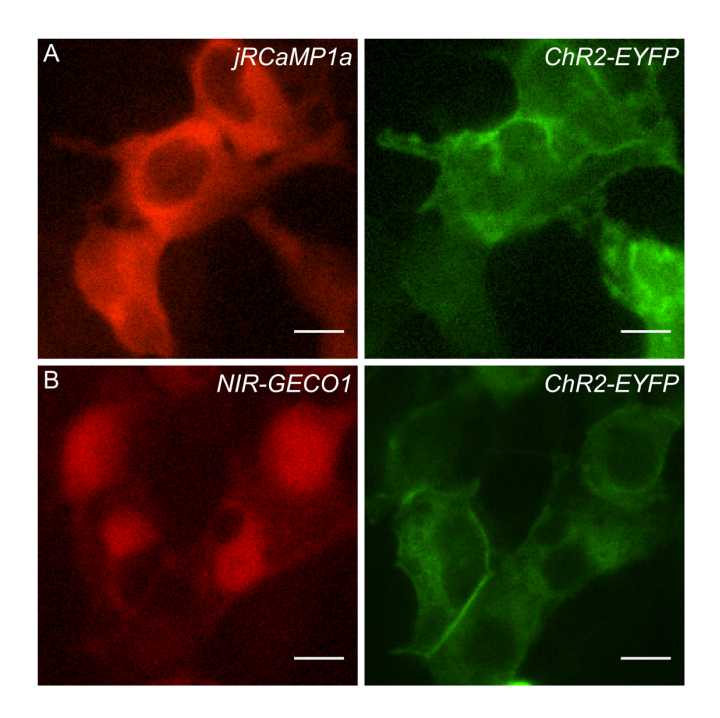


Figure S1. Co-expression of *ChR2* with *jRCaMP1a* or *NIR-GECO1* in HEK 293 cells (related to Figure 1).

Example fluorescence images of *ChR2-jRCaMP1a* (A) and *ChR2-NIR-GECO1* (B) co-expressed cells, pseudo-colored with light red for *jRCaMP1a*, deep red for *NIR-GECO1* and green for *ChR2-EYFP*. Scale bar, 10 μm.

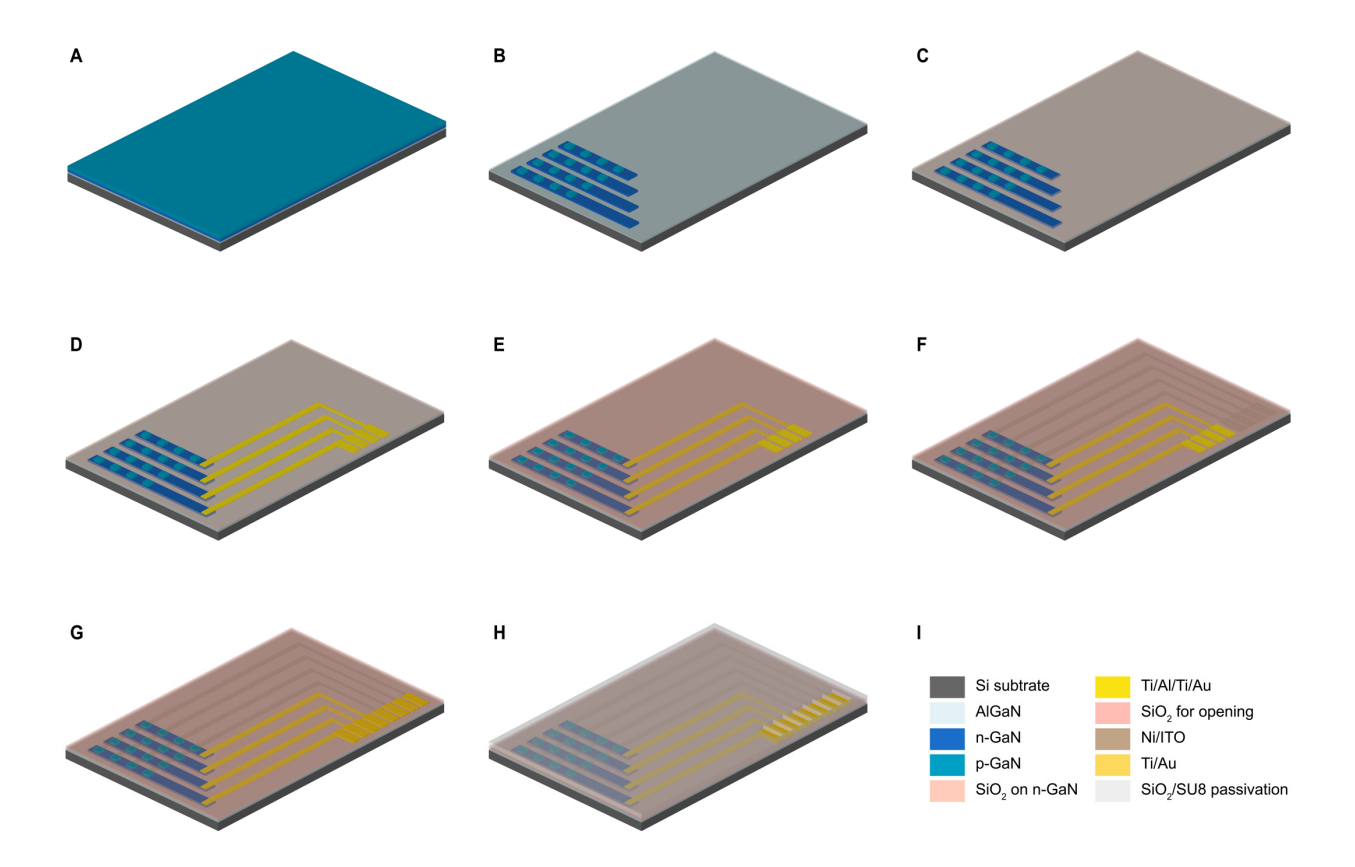


Figure S2. Fabrication flow of the micro-LED array (related to Figure 1). On an epitaxial GaN-on-Si wafer (A), LED pixels were defined by two RIE steps (B). Four n-GaN islands were passivated by a PECVD based SiO₂ layer (PECVD-SiO₂) (C), followed by evaporating Ti/Al/Ti/Au layers as the n-contact (D). The array was then passivated by a second PECVD-SiO₂ layer, followed by a RIE step to open the pixels and pad areas (E). Next, Ni/ITO (F) and Ti/Au (G) layers were made as p-contact and pad contact, respectively. The entire array was finally encapsulated by PECVD-SiO₂/SU8 layers (H).

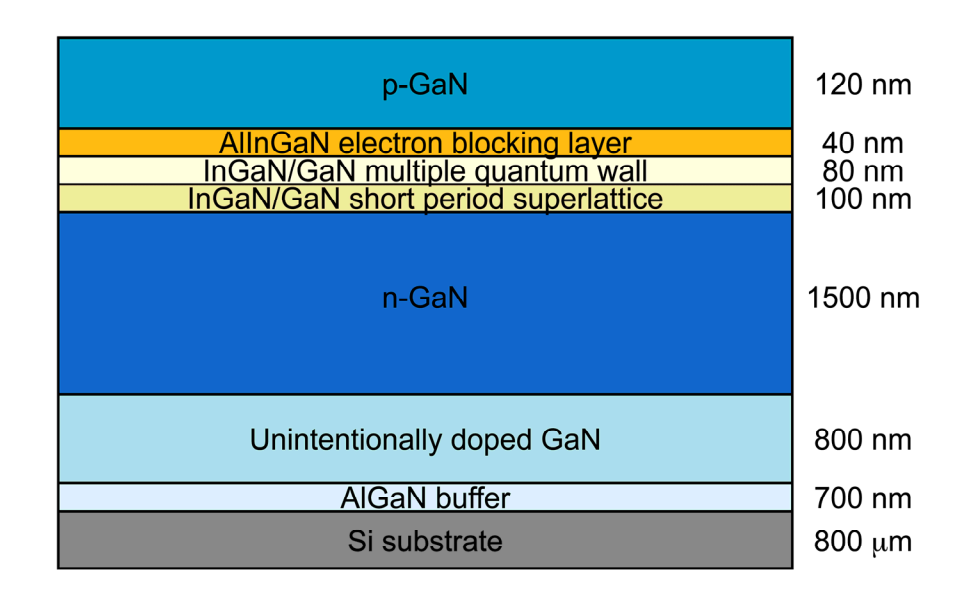


Figure S3. Cross-sectional view of a GaN-on-Si wafer (related to Figure 1).

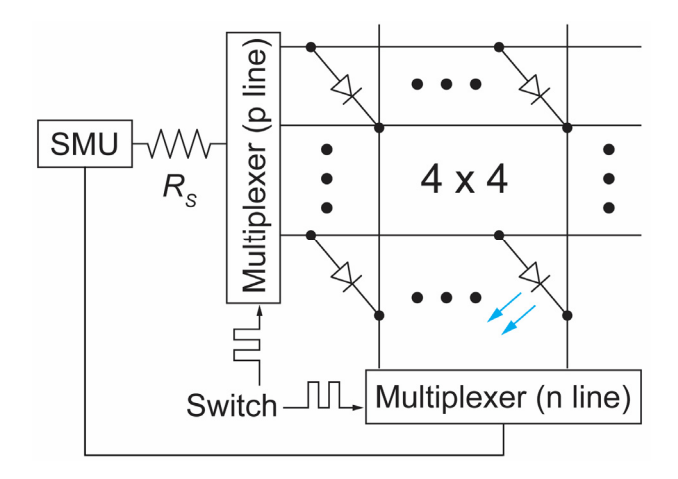


Figure S4. Off-board multiplexing circuit to access individual pixels in a 4-by-4 micro-LED array (SMU: source-measurement unit). $R_{\rm S}$ represents the applied series resistor (related to Figure 1).

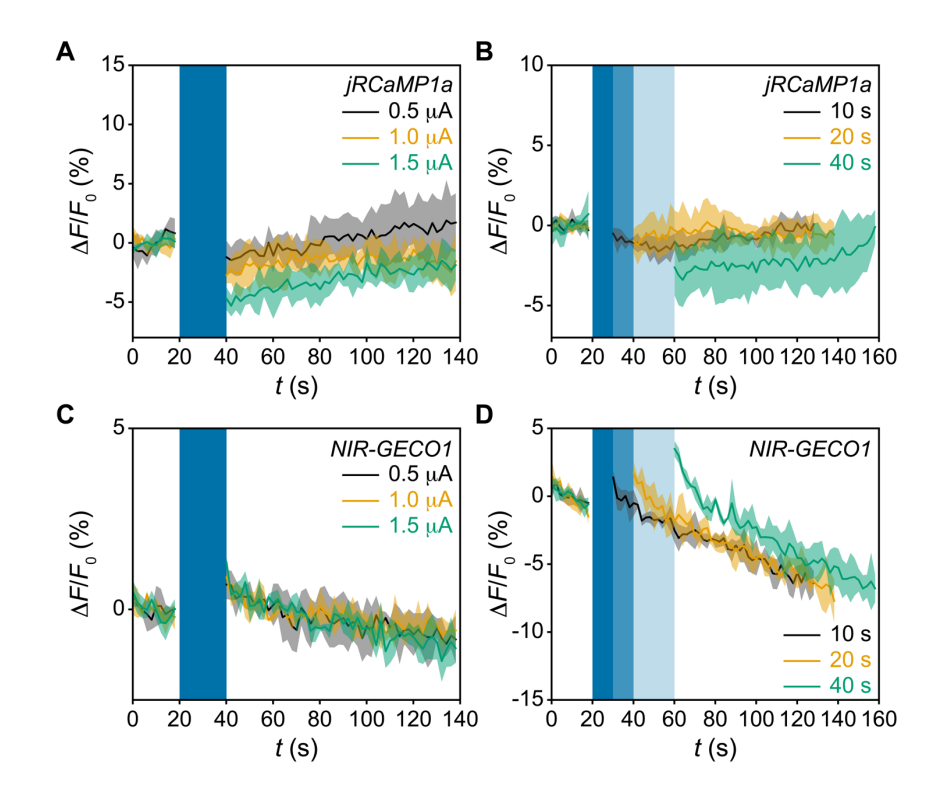


Figure S5. Control cell responses to optogenetic stimulus offered by LEDs (related to Figure 3). (A) $\Delta F/F_0$ traces from a jRCaMP1a control cell with T_{LED} = 20 s and I_{LED} ranging from 0.5 to 1.5 μ A. (B) $\Delta F/F_0$ traces from a jRCaMP1a control cell with T_{LED} ranging from 10 to 40 s and I_{LED} = 1.5 μ A. (C) $\Delta F/F_0$ traces from a NIR-GECO1 control cell with T_{LED} = 20 s and I_{LED} ranging from 0.5 to 1.5 μ A. (D) $\Delta F/F_0$ traces from a NIR-GECO1 control cell with T_{LED} ranging from 10 to 40 s and I_{LED} = 1.5 μ A. Blue windows represent the periods of optogenetic stimulus; solid lines represent the mean value from three consecutive recording periods; shaded areas represent ± 1 s.d.

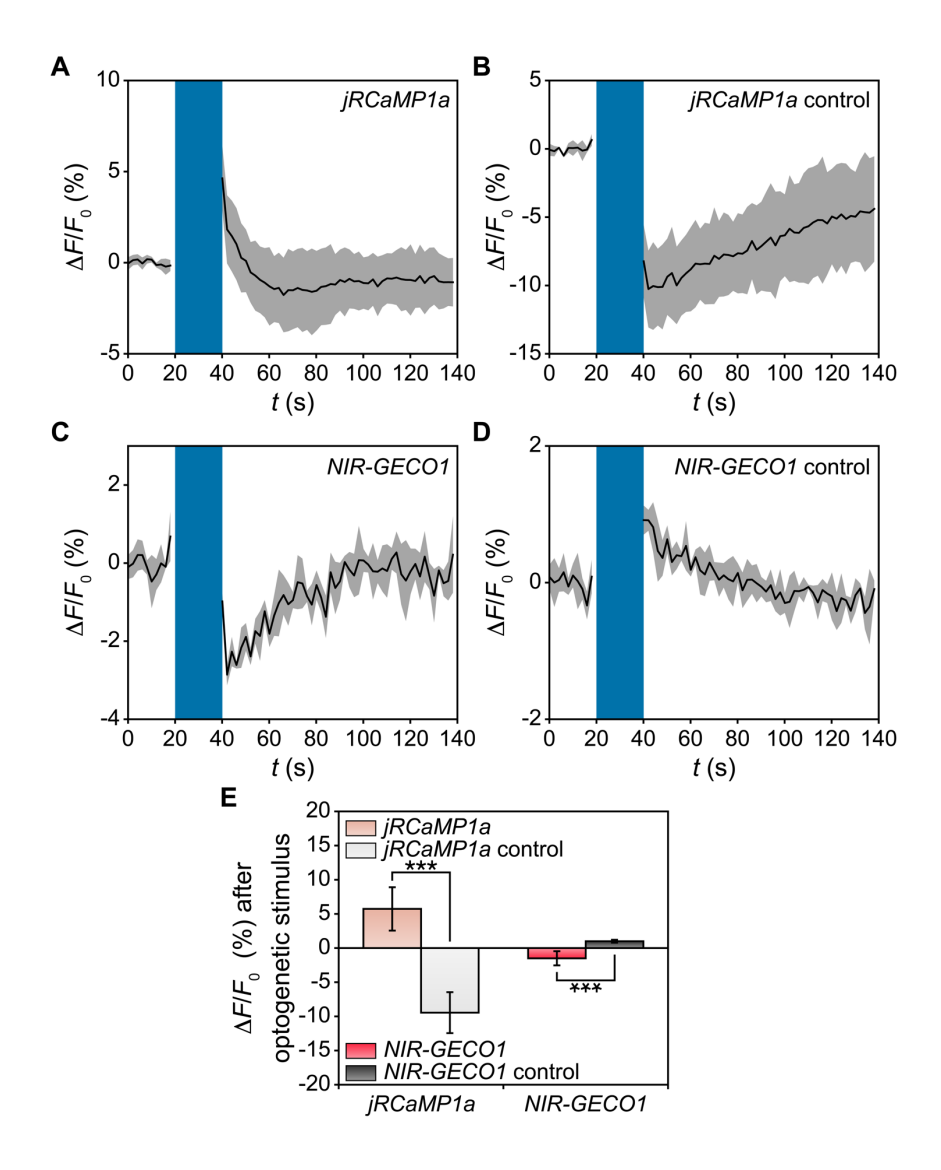


Figure S6. Cell responses to optogenetic stimulus offered by a fluorescence microscope (related to Figure 3).

Representative $\Delta F/F_0$ traces with 20 s microscope-based optogenetic stimulus from a ChR2-jRCaMP1a co-expressed cell (A), a jRCaMP1a control cell (B), a ChR2-NIR-GECO1 co-expressed cell (C), and a NIR-GECO1 control cell (D). In A, B, C, and D, blue windows represent the periods of optogenetic stimulus; solid lines represent the mean value from three consecutive recording periods; shaded areas represent ± 1 s.d. (E) Statistical analysis of $\Delta F/F_0$ signals. Error bars represent ± 1 s.d. (n = 15 from 5 independent cells in each group, 3 recording periods from each cell); ***P < 0.001 based on Student's t-test.

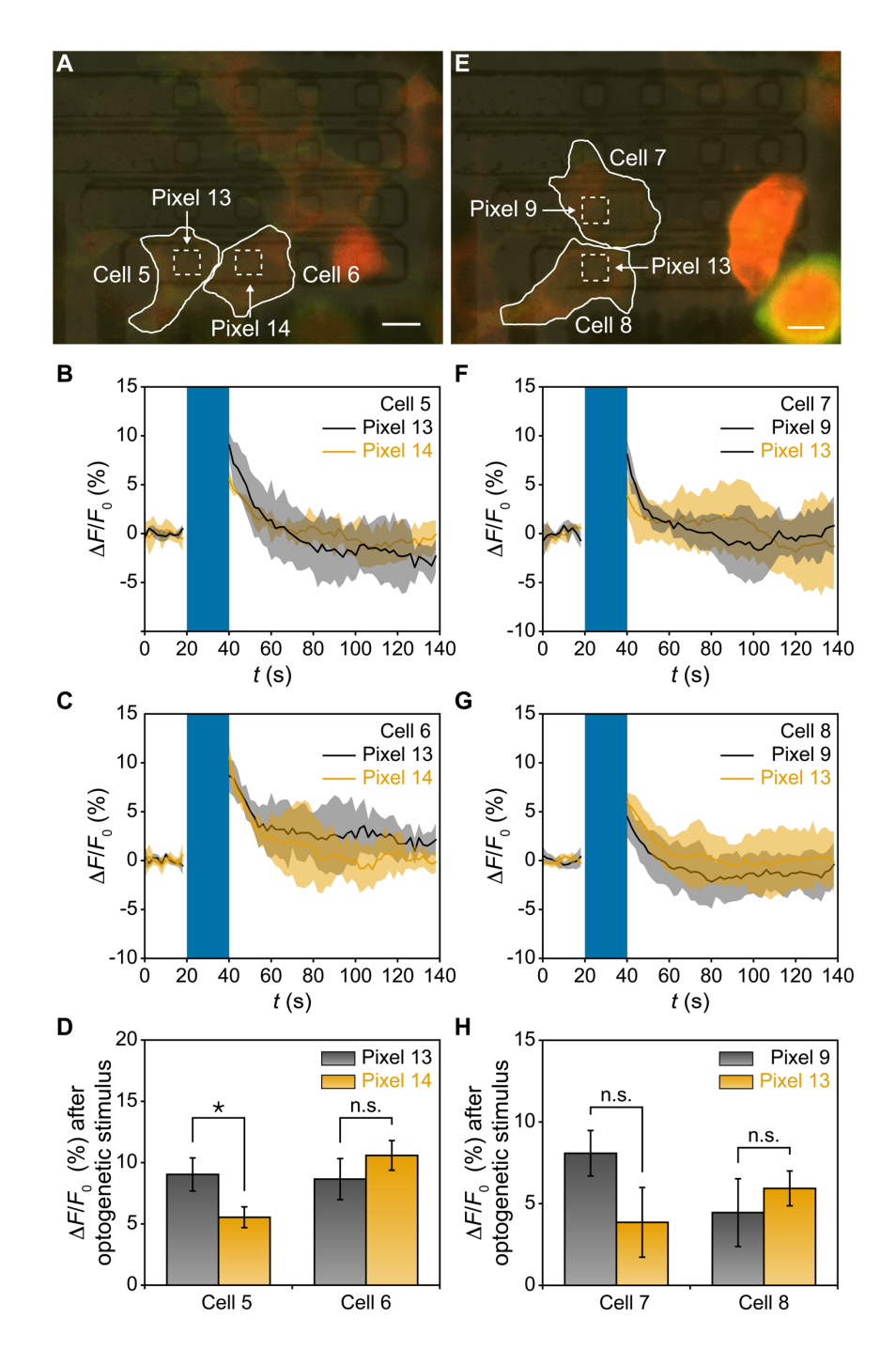


Figure S7. Additional two experiments to evaluate the spatial resolution of the optogenetic stimulus offered by LEDs (related to Figure 4).

(A) One pair of cells (outlined, overlapped with pixels 13 and 14) were sub-1 μ m apart. Scale bar, 10 μ m. (B) $\Delta F/F_0$ traces from cell 5 that was stimulated by pixels 13 and 14 with T_{LED} = 20 s. (C) $\Delta F/F_0$ traces from cell 6 that was stimulated by pixels 13 and 14 with T_{LED} = 20 s. (D) Statistical analysis of $\Delta F/F_0$ signals from cell 5 and cell 6. (E) Another pair of cells (outlined, overlapped with pixels 9 and 13) were sub-1 μ m apart. Scale bar, 10 μ m. (F) $\Delta F/F_0$ traces from cell 7 that was stimulated by pixels 9 and 13 with T_{LED} = 20 s and $P_{light} \sim 0.71$ mW/mm². (G) $\Delta F/F_0$ traces from cell 8 that was stimulated by pixels 9 and 13 with T_{LED} = 20 s and $P_{light} \sim 0.71$ mW/mm². (H) Statistical analysis of $\Delta F/F_0$ signals from cell 7 and cell 8. In B, C, F, and G,

blue windows represent the periods of optogenetic stimulus; solid lines represent the mean value from three consecutive recording periods; shaded areas represent ± 1 s.d. In D and H, error bars represent ± 1 s.d. (n = 3 recording periods); *P < 0.05, n.s. P > 0.05 based on Student's t-test. The t_{LED} values applied to output t_{light} ~ 0.71 mW/mm² were 1.6 t_{LED} has for pixel 9,1.0 t_{LED} has for pixel 13, and 1.1 t_{LED} has results suggest that our array cannot address individual cells that are sub-1 t_{LED} has a part.

Transparent Methods

1. Array fabrication.

GaN-on-Si wafers (Enkris Semiconductor) were formed by sequentially growing a AlGaN buffer layer (700 nm), an unintentionally-doped GaN (800 nm) layer, a Si doped n-GaN layer (1500 nm), a InGaN/GaN short period superlattice layer (100 nm), a quantum well layer (80 nm), a AllnGaN electron blocking layer (40 nm), and a Mg-doped p-GaN layer (120 nm) on top of a (111) Si substrate (800 μ m). Our LED pixels were defined by two RIE steps. A PECVD-SiO₂ (~200 nm) layer was first applied to passivate n-GaN islands, followed by evaporating Ti/Al/Ti/Au (10/70/10/120 nm) layers as the n-contact. The array was then passivated by a second PECVD-SiO₂ (~200 nm) layer, followed by a RIE step to open the pixel- and pad-areas, as well as a 10-s dip in 50:1 buffered oxide etchant to remove residual SiO₂ (if any). Next, exposed p-GaN areas were treated by a dilute HCl solution (10%) for 30 s to etch unintentionally oxidized, if any, GaN regions, and contacted by sputtered Ni/ITO (5/120 nm) layers. Afterwards, Ti/Au (10/200 nm) layers were deposited to create the pad contact. The entire array was then annealed at 500 °C for 5 mins in an O₂ atmosphere (20 sccm, 120 mtorr) to reduce the contact resistance. Finally, the array was encapsulated by PECVD-SiO₂ (~200 nm)/SU8 (14 μ m) layers before the cell experiment.

2. Cell seeding on PDMS pieces.

PDMS pieces were prepared with a ~200 μ m thickness according to the manufacturer's recommendation. Before cell seeding, each PDMS piece was sterilized by 30-minute ultrasonication in 70% ethanol, dried with compressed air, and placed in a 48-well plate (Fisher Scientific). To improve the cell adhesion, we applied a 7-min UV-Ozone treatment (MODEL30, Jelight) to activate the PDMS pieces, coated them with fibronectin (50 μ g/ml in DI water, ThermoFisher) for 1 hr at room temperature, and applied 3 times of 1X phosphate buffered saline (ThermoFisher) wash.

After these steps, HEK 293 cells (ATCC CRL-3216) were passaged by 0.25% trypsin (ThermoFisher) and seeded onto the PDMS pieces at a density of 20,000 cells/cm². Cells were cultured in 90% Dulbecco's Modified Eagle Medium (high glucose, no glutamine) (ThermoFisher), supplemented by 10% Fetal Bovine Serum (Sigma-Aldrich), 1% penicillin/streptomycin (ThermoFisher), 1% GlutaMAX (100X, ThermoFisher) and 1% Sodium Pyruvate (100 mM, ThermoFisher), and kept in a humidified incubator (ThermoFisher) at 37 °C with 5% CO₂.

3. Plasmid purification and cell transfection.

The plasmids encoding *ChR2*, *jRCaMP1a*, and *NIR-GECO1* we used are *pcDNA3.1/hChR2(H134R)-EYFP* (Addgene #20940), *pGP-CMV-NES-jRCaMP1a* (Addgene #61562) and *pDuEx2-NIR-GECO1* (Addgene #113680), respectively. Bacteria containing these plasmids were first cultured in LB Agar plates (added with kanamycin or ampicillin) at 37 °C overnight. Afterwards, single colonies were picked and cultured in LB broth with agitation at 37 °C overnight to amplify the number of plasmids. Finally, plasmids were purified by a HiSpeed Plasmid Midi Kit (QIAGEN) according to the manufacturer's recommendation.

Cell culture medium was refreshed with addition of 2 μ M *all-trans-retinal* (Sigma-Aldrich) 12~24 hours after cell seeding when cell culture reaches 60-70% confluency. Cells were then transfected by adding 40 μ L 1 X OPTI-MEM (ThermoFisher) solution mixed with 200 ng of each plasmid (either with single plasmids or one pair of plasmids for co-transfection) and 0.5 μ L Lipofectamine LTX reagent (ThermoFisher) to each well of the 48-well plate.

4. Ca2+ imaging under optogenetic stimulus.

Ca²⁺ imaging of HEK 293 cells under optogenetic stimulus was performed 24~48 hours after transfection, with an imaging solution containing 80 mM CaCl₂, 20 mM glucose, 23 mM NMDG, 5 mM NaCl, 3 mM KCl, 1 mM MgCl₂, and 10 mM HEPES (pH 7.3). Cell experiments were conducted using an epifluorescence upright microscope (FN1, Nikon) equipped with a Zyla4.2 plus sCMOS (scientific complementary metal-oxide semiconductor) camera (Andor, USB 3.0) and a SPECTRA X light engine (Lumencor). Cells were

imaged with a CFI6O Fluor 20× water immersion objective lens (NA = 0.5, Nikon) at room temperature. Specifically, we applied: (1) a 6.2 mW 575/25 nm excitation light, a 585 nm long-pass dichroic mirror, and a 632/60 nm emission filter to image *ChR2-jRCaMP1a* co-expressed and *jRCaMP1a* control cells; (2) a 23.1 mW 640/30 nm excitation light, a 660 nm long-pass dichroic mirror, and a 665 nm long pass emission filter to image *ChR2-NIR-GECO1* co-expressed and *NIR-GECO1* control cells; (3) a 3.92 mW 470/24 nm excitation light, a 495 nm long-pass dichroic mirror, and a 520/40 nm emission filter to examine the *ChR2* expression by EYFP imaging. Optogenetic stimulus was offered by either micro-LEDs or a 3.92 mW 470/24 nm light from the SPECTRA X light engine. Fluorescence was sampled at 0.5 frame per second (100 ms exposure time per frame, no binning). The micro-LED array was current biased using a B2902A source-measurement unit (Keysight), which was triggered by FN1 to synchronize with the camera. The microscope-based stimulus was synchronized with the camera using Nikon-Elements Advanced Research software (Nikon).

5. Device characterization.

LED pixels were biased at $I_{LED} = 0.1 - 2$ μA at a step of 0.1 μA by Keysight B2902A, with a 400 kΩ series resistor (R_S) applied to protect the array damage due to improper voltage levels. Accordingly, the V_{LED} values in measured I-V curves were corrected by subtracting the voltage drop across R_S . During the pulsing test, the select pixel was pulsed at $I_{LED} = 2$ μA with a 10 ms-duration; I_{light} of the select pixel was recorded by FN1 for one second (1 ms exposure time per frame, no binning or filter cube was applied).

Optical power of micro-LEDs was measured by a digital optical power and energy meter console (PM100D, Thorlabs) connected with a photodiode power sensor (s120C, Thorlabs). The wavelength correction of the power meter was set to 462 nm to match the dominant photoluminescence wavelength of as-made micro-LEDs. Spatial profile of the output light was also captured by FN1 with 1 ms exposure time per frame (no binning or filter cube was applied).

6. Statistical significance.

Statistical analysis in Figs. 3, 4, S6, and S7 was based on Student's *t*-test (two-tailed, independent two-sample *t*-test).